First principle investigation of the structural, electronic and optical properties of methylammonium lead iodide: implications for photovoltaic applications

Arti Meena, Sarita Kumari* and Amanpal Singh

Department of Physics,
University of Rajasthan,
Jaipur, 302004, India
Email: arti20381@gmail.com
Email: sarita.kumari132@gmail.com
Email: amanbkh@gmail.com
*Corresponding author

Ajay Singh Verma

Department of Physics,
Banasthali Vidyapith,
Niwai, Tonk, 304022, India
Email: ajay_phy@rediffmail.com

Abstract: In the present work structural, electronic and optical properties of methylammonium lead iodide have been investigated by full potential linearised augmented plane wave (*FP–LAPW*) method with the local density approximation. The structural properties; lattice constants, bulk modulus and derivative of bulk modulus are calculated. The direct energy band gap of is found to be 1.52 eV at an R-R point which makes the material suitable for photovoltaic applications. The optical properties; dielectric function, extinction coefficient, refractive index, absorption coefficient, reflectivity, electron energy loss function and photoconductivity of $CH_3NH_3PbI_3$ are discussed and the analysis confirms reliability of $CH_3NH_3PbI_3$ material for the solar cell absorption layer.

Keywords: first principle study; perovskite; structural; electronic and optical properties.

Reference to this paper should be made as follows: Meena, A., Kumari, S., Singh, A. and Verma, A.S. (2021) 'First principle investigation of the structural, electronic and optical properties of methylammonium lead iodide: implications for photovoltaic applications, *Int. J. Computational Materials Science and Surface Engineering*, Vol. 10, No. 1, pp.27–45.

Biographical notes: Arti Meena is a Research Scholar in Condensed Matter Physics at Department of Physics, University of Rajasthan, Jaipur. She received her Bachelor's degree in Science from Kota University and a master's degree in Physics from The IIS University, Jaipur.

Sarita Kumari is currently working as an Associate Professor in Department of Physics, University of Rajasthan, and Jaipur. She has 23 publications with 86 citations. Her current interests are modelling and development of organic-inorganic solar cell, image processing (wavelet analysis).

Amanpal Singh is currently working as an Assistant Professor in Department of Physics, University of Rajasthan, and Jaipur. He is MSc in Physics, PhD in Thin Films Technology, he has 25 publications with 184 citations. His current interests are wide band gap semiconductors, thin film and green energy technologies.

Ajay Singh Verma is MSc in Physics and PhD, he has a 119 publications with 931 citations.

1 Introduction

In the recent few years, perovskite photovoltaic technologies have been emerging as a suitable candidate capable of developing photovoltaic properties with high efficiency and performance (Kojima et al., 2009; Kim et al., 2012; Yang et al., 2017). The organometallic lead halide perovskite materials in solar cell application have produced remarkable growth (Ponseca et al., 2014; Gao et al., 2014; Wang et al., 2014; Najafi et al., 2018; Huang et al., 2020; Bing et al., 2019; Singh et al., 2019),(Bing et al., 2019),(Yun et al., 2018). They have proved the advantages over conventional silicon and GaN based solar cells, such as flexibility, low cost and ease of fabrication (Kumar et al., 2013). Their room temperature processing and earth abundant elemental constitution makes them advantageous over other thin film absorber materials (Prakash Singh and Nagarjuna, 2014; Kulkarni et al., 2014). Also, they have s–p anti-bonding coupling which provides strong optical absorption. They have unique electronic properties which involve higher electron and hole mobility, high carrier diffusion lengths and low surface recombination velocity. The structural properties involve tolerance to structural defect and shallow point defects as well as low grain boundary effects (Hao et al., 2014; Umebayashi et al., 2003; Mosconi et al., 2013; Umari et al., 2014). These properties are attributed to nature of perovskite lattice and make them suitable for optoelectronic applications (Hagfeldt et al., 2010; Chen et al., 2003). The hybrid organic–inorganic nature of halide perovskites due to replacement of inorganic cation with the organic one, in perovskite lattice make them superior than the previously developed dye-sensitised solar cells, organic PVs, and other popular thin film material systems (Onoda-Yamamuro et al., 1990; Shah et al., 2014; Juarez-Perez et al., 2014; Lind et al., 2011).

A family of most efficient lead halide perovskite having the general formula is ABX_3 can be described (Figure 1) where A is a large sized cation (organic such as $CH_3NH_3^+$), E is a small sized metallic cation (Pb^{2+}), and I is halide ions which binds to both cations.

Figure 1 Typical structures for ABX_3 perovskites: (a) Ball-and-stick representation of $CH_3NH_3PbX_3$ (X = Br/I); Pb atoms are represented by the dark spheres inside the octahedral; the *I*/Br atoms are purple spheres at the octahedral corners; CH_3NH_3 molecule is inside the cuboctahedral cavity; PbX_6 is shown as black octahedral; (b) Ball-and-stick representation and (c) two time in a number of atoms in a single unit cell (2 * 2 * 2) (see online version for colours)

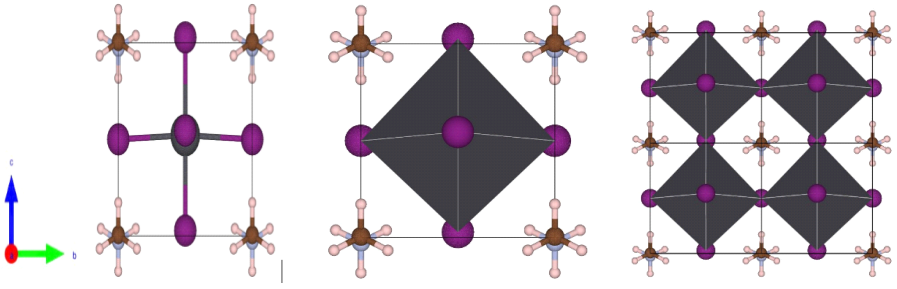

(a) (b) (c)

The perovskite structure is not ideally cubic, it is slightly distorted. This distorted perovskite material exhibits many properties such as superconductivity, ferromagnetism, ferroelectricity, and multiferrocity. The properties of these materials can be modified for their application in photovoltaic devices. For this we need to develop computational techniques that can describe their electronic structure accurately and the first-principles calculations are one of the most powerful tools for finding important physical and chemical properties of materials with great accuracy.

In this connection, density functional theory has been used to describe electronic structures of $CH_3NH_3PbX_3$ (X = Cl, Br, I) and $CH_3NH_3PbI_2X$ (Mosconi et al., 2013; Umari et al., 2014). Also, electronic properties of Cs-doped $CH_3NH_3PbI_3$ by first-principles calculations are predicted and found that $CH_3NH_3PbI_3$ has a direct band gap of 1.68 eV, and 12.5% Cs doping increases the band gap of 1.73 eV (Liu et al., 2018). Radi A. Jishi calculated band structure of $CH_3NH_3PbI_3$ using the mBJ potential and the band gap found to be 1.55eV (Jishi et al., 2014).

Further, in practical applications, organometallic halide perovskite solar cells suffer from environmental stability due to water, light, heat. Also, ionic instability occurs due to changes in the stable tetrahedron structure of BX_3 due to inclusion of organic ion (Liu et al., 2018). This instability can be reduced by structural optimisation of ABX_3 which involves the minimisation of energy as a function of volume using first principles calculations.

Here we focus on $CH_3NH_3PbI_3$ perovskite materials for first principle calculations to know their structural, electronic, optical and mechanical properties within the frame of density functional theory. Estimation of these properties will be helpful to check suitability of these materials as an absorption layer in the solar cell structure. Stability of perovskite structure is discussed with calculation of octahedral tolerance factor,

Goldsmith tolerance factor and formation energy. Moreover, structural properties of $CH_3NH_3PbI_3$ are compared with that of $CH_3NH_3PbBr_3$ to understand the effect of halide ions over stability of methylammonium lead halide perovskite materials.

2 Methods

The selection of materials for photovoltaic applications can be done on the basis of their electronic and optical properties. The understanding of the origin of these properties of ABX_3 materials can provide a step forward for their uptake in photovoltaic industry. A first principle calculation approach is a reliable method for calculating structural, electronic, optical as well as mechanical properties of materials. The method of choice is ideally *FP–LAPW* computational scheme (Madsen et al., 2001; Schwarz et al., 2002) as implemented in the *WIEN2k* code (Blaha et al., 2019). In this scheme Kohn-Sham (KS) equations are solved within the framework of density functional theory (DFT) to find the ground state density and total energy. All the physical properties of materials are dependent on energy density, so it is necessary to minimise energy for a stable structure. The minimisation of energy as a function of cell volume provides equilibrium lattice constants for the stable structure. (Wu and Cohen, 2006).

Further local density approximation (LDA) (Tran et al., 2007) and generalised gradient approximation (GGA) (Perdew et al., 1996) are the popular methods for solving the Kohn-Sham (*KS*) equation. In LDA the electronic and magnetic properties of the strongly correlated systems are not justified appropriately. The GGA approximations include up to semi-core correction, which can provide more accurate results during DFT simulations. However, we use LDA approximation for the calculation due to its simplicity.

For the solution of KS equations the space is divided into two parts; one is a muffin tin (MT) sphere and another is interstitial region. The FP–LAPW method provides an expansion of KS orbitals as plane waves in the interstitial region, but inside the muffin tin spheres expansion is in terms of atomic like orbitals. The radii (bohr) of the muffin-tin spheres are 25 for Pb and Br/I, 1.18 for *N*, 1.24 for *C*, and 0.64 for *H*. Inside the muffin-tin spheres, the spherical harmonics considered is $l_{\max} = 10$. As the *MT* radius of hydrogen atoms is quite small i.e., $R_H = 0.64$; the expansion of KS orbitals in the interstitial regions is set for $R_H K_{\max} = 3$, Monkhorst-Pack scheme (Monkhorst and Pack, 1976) with $5 \times 5 \times 5$ grids is used for k-point sampling of the Brillouin zone. The total energy tolerance of 10^{-6} Ry is taken for convergence of the self-consistent calculations.

3 Results and discussion

3.1 Structural properties

The ABX_3 cubic perovskite structure consists of a simple cubic unit cell, *E* atoms are placed at the cube corners with the six halogen atoms coordinated octahedrally. The hinged octahedral allows several sets of cooperative rotations, known as tilt transitions, promote symmetry, providing a variety of wide adjustments of B–X–B bond angle

showing different structures at different temperatures. Experimentally it has shown that $CH_3NH_3BX_3$ compound may exist in three different phases in different temperature range. This compound exists in orthorhombic phase at low temperature, tetragonal at medium temperature and pseudo-cubic at high temperature (Feng, 2014).

Here, for simplicity of calculations, we take into consideration only the cubic phase and structural, optical and electronic properties of lead halide perovskite material are discussed. In order to find the structural properties, the optimisation of lattice constants and atomic positions is done by minimising the total energy as a function of volume. Also by fitting Energy Volume (E-V) curve with Murnaghan equation (Tyuterev and Vast, 2006) (Figure 2), we get the information about the structural properties of $CH_3NH_3PbX_3$ (X=*Br/I*) compound. The structural properties calculated in LDA approximation are presented in Table 1(a) and (b) along with the comparison of available experimental and other theoretical results. Theoretically reported value of the lattice constant of $CH_3NH_3PbI_3$ is a = 6.38A° (Poglitsch and Weber, 1987) and $CH_3NH_3PbBr_3$ is a = 5.92A° (Weber, 1978) and the calculation by LDA approximations confirms the value 6.3739A° and 5.872A°respectively. The calculated lattice constant of the present work is slightly different than the other theoretical value due to difference in method of calculation. Moreover the values are closer to the experimental result which confirms the reliability of the present method. Also, in the absence of available experimental value for bulk modulus, no comparison is possible here.

Table 1 Structural equilibrium parameters; lattice constant $a(A°)$, unit cell volume $V(A°)^3$, Bulk modulus $B(GPa)$ and derivative of bulk modulus $B'(GPa)$ for $CH_3NH_3PbX_3(X = Br, I)$

(a)

Properties ($CH_3NH_3PbI_3$)	*This work*	*Other calculations*	*Expt.*
$a(A°)$	6.3739	6.30[a], 6.2621[b], 6.38[c,d]	6.3285[e],6.28[f], 6.33[e]
$V(A°)^3$	258.94	248.4[a]	253.5[e] ,251.60[g]
B(GPa)	38.1627	16.4[a]	–
B′(GPa)	3.6905	–	–

[a]Feng (2014), [b]Indari et al. (2017), [c]Kim et al. (2014), [d]Egger and Kronik (2014), [e]Poglitsch and Weber (1987), [f]Baikie et al. (2013) and [g] Stoumpos et al. (2003).

(b)

Properties ($CH_3NH_3PbBr_3$)	*This work*	*Other calculations*	*Expt*
$a(A°)$	5.872	5.933[h]	5.92[i]
$V(A°)^3$	202.52	225[j]	206.3[k]
B(GPa)	51.181	–	–
B′(GPa)	4.0103	–	–

[h]Jishi et al. (2014), [i]Weber, 1978), [j]Roknuzzaman et al. (2018) and [k]Ryu et al. (2014).

Figure 2 Total energy vs. volume curve with LDA approximation: (a) $CH_3NH_3PbI_3$ and (b) $CH_3NH_3PbBr_3$ (see online version for colours)

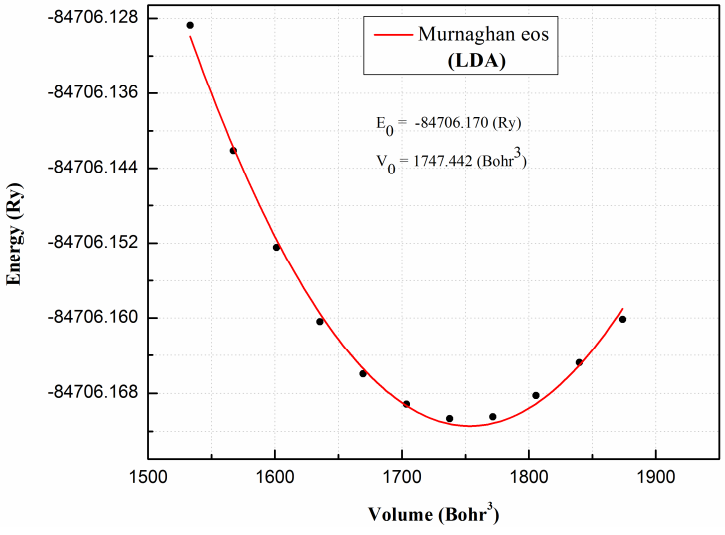

(a)

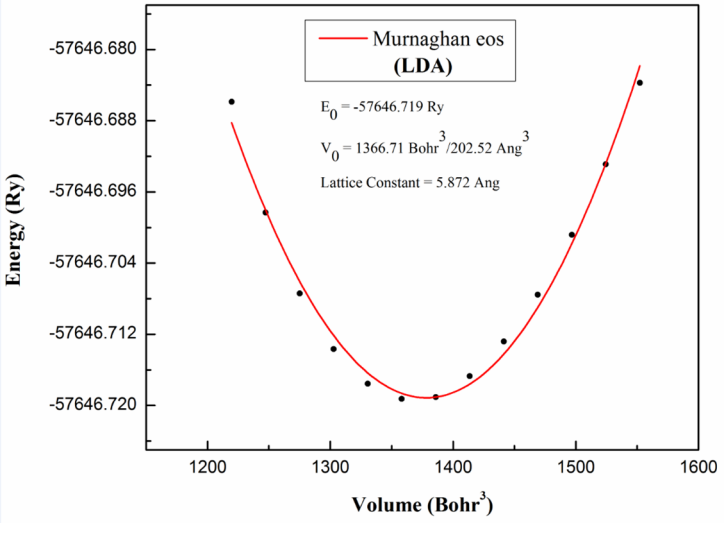

(b)

3.2 Electronic properties

3.2.1 Band structure curves

Different orientations of A, B and X in ABX_3 perovskites introduce change in internal degree of freedom which in turn is responsible for variation in energy of electronic structure.

The important information about crystal structure can be obtained from band structure curves. The band structure diagram of cubic $CH_3NH_3PbI_3$perovskite with *LDA* and *GGA* approximation is shown in Figure 3. Here the energy function is plotted for the first Brillouin zone. The band gap value is found by the difference in energies of valence band maximum (VBM) and conduction band minimum (CBM). Figure 3 shows that the compound is a semiconductor having a direct band gap of 1.52 eV with *LDA* and 1.488 with *GGA*. However the experimental results are reported as 1.51 eV and 1.58 eV (as shown in Table 2) (Shi et al., 2015; Tonui et al., 2018). This shows good agreement in between calculated and experimental results using with *LDA* approximation. Here the results slightly differ from the experimental one as the calculations are done for ground state, whereas in the experimental results there is also a contribution of excited states with higher energies (Afsari et al., 2016). This in turn makes the calculated values of band gap lower than the experimental one. Moreover, the other symmetry points are also obvious in band energy curve; which are the *M* symmetry point and Γ symmetry point with energy values 1.76 eV and 2.71 eV respectively. Further, it is observed that the conduction band is more dispersive than the valence band because it is delocalised due to transition of electrons to the higher energy states.

Figure 3 Band structure of cubic phase of $CH_3NH_3PbI_3$ perovskite with: (a) LDA approximation and (b) GGA approximation (see online version for colours)

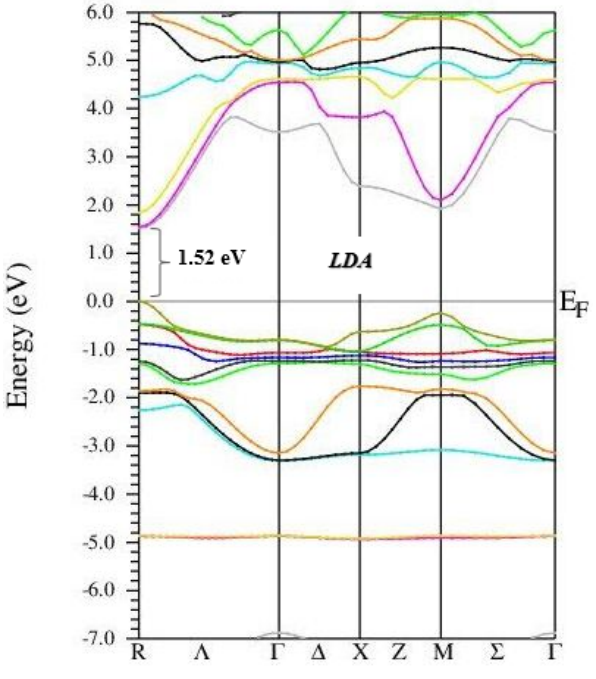

(a)

Figure 3 Band structure of cubic phase of $CH_3NH_3PbI_3$ perovskite with: (a) LDA approximation and (b) GGA approximation (see online version for colours) (continued)

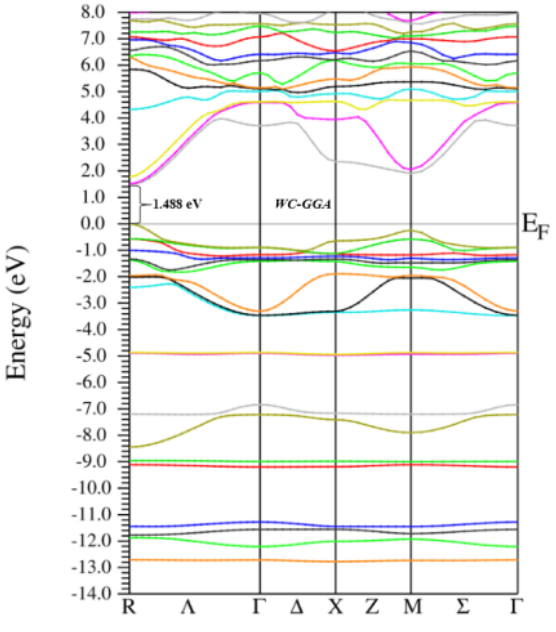

(b)

Table 2 Calculated band gap with LDA and GGA approximation and comparison with other theoretical and experimental data

Method of approximation	*E_g (theoretical)*	*E_g (experimental)*	*Deviation from experiment (%)*
LDA	1.52 [This work]	1.51[h]	0.66%
GGA	1.48 [This work]	1.58[i]	3.79%`
		1.55[j,k]	1.93%
PBE	1.55[l]		
PBE/HSE+SOC	1.50[m]; 1.53[n]	–	–
GGA	1.50[o]	–	–
PBE sol	1.44[p]	–	–

[h]Shi et al. (2015), [i]Tonui et al. (2018), [j]Kojima et al. (2009), [k]Ogomi et al. (2014), [l]Mosconi et al. (2013), [m]Amnuyswata and Thanomngam (2017), [n]Yin et al. (2015), [o]Yin et al. (2014) and [p]Thind et al. (2017).

3.2.2 Density of states (DOS)

According to Figure 4, the total density of states is divided into three different regions; lower valance band (–5.5 eV to –3.5 eV), upper valance band (–3.5 eV to 0 eV) and lower conduction band. The region of the lower valence band mainly consist of MA–p orbitals. The upper valence band (UVB) is mainly contributed by weak hybridisation of *I*–5*p* with *Pb*–5*s* and *Pb*–6*p* state. The last region, the lower conduction bands (LCB) is mainly formed by hybridisation of *I*–5*p* and *Pb*–6*p* orbital.

Figure 4 The density of states of $CH_3NH_3PbI_3$ perovskite (see online version for colours)

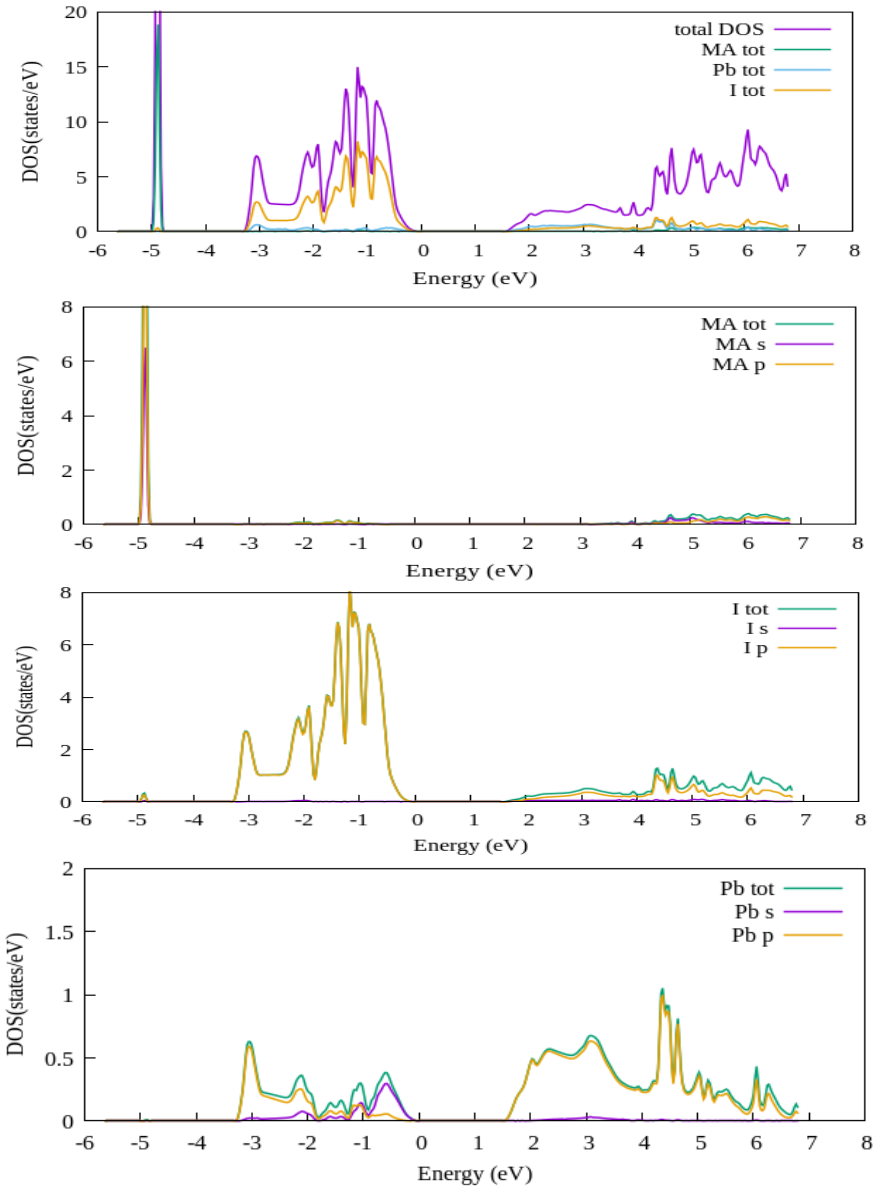

These interpretations show that the band gap of $CH_3NH_3PbI_3$ is strongly correlated with the structure of inorganic molecules i.e., PbI_6 octahedral. Thus the origin of electronic properties of seeming to be a distortion of octahedral rather than any direct contribution of the group in the electronic structure (Liu et al., 2018). This distortion in PbI_6 octahedral arises due to the size and orientation of $(CH_3NH_3)^+$ according to Jahn–Teller effect (Tonui et al., 2018). As the electronic and optical properties are being tailored by the change in orientation of PbI_6 octahedral only, this fact feature about electronic

structure can be helpful in improving the stability of the material through the element substitution with inorganic octahedral. As with this substitution, electronic properties may remain unaltered, the stability of the absorber layer in solar cell may be improved without affecting conversion efficiency.

3.2.3 Structural stability

The stability of perovskite structure can be investigated by Goldschmidt tolerance factor (Goldschmidt, 1926), which is given as:

$$t = (r_A + r_x) / \sqrt{2(r_B + r_x)} \tag{1}$$

Here r_A is the radii of organic group, r_B is the radii of metal ion and r_x is the atomic radii of halogen ion, $t = 1$ (ideal tolerance factor) provides a perfect cubic lattice, whereas most stable perovskite structures with tetragonal, orthorhombic and trigonal lattices are determined by $0.8 \leq t \leq 1.0$. In ABX_3 structure cation A is too large for $t > 1$ and is too small for $t < 0.8$, which leads to non-perovskite structure (Bartel et al., 2019). In general, the value of t in between 0.9 to 1 be considerable for highly stable structure. Though the criteria is developed for organic perovskite structure, is still valid for organic inorganic hybrid metal halide perovskites.

Since the change in band structure arises due to inclusion of organic ion in stable octahedral structure. The stability can be measured in terms of another constant, which is known as octahedral factor. This factor is defined as ratio of r_B and r_x (Bartel et al., 2019),

$$\mu = r_B / r_X \tag{2}$$

If μ is smaller than 0.414, low coordination number leads to unstable octahedral structure, whereas slightly greater than 0.414 values of μ shows the contact of B cation with six X anions leading to a stabilise the BX_6 octahedral structure. The stability can be confirmed with the criteria; $0.414 \leq \mu < 0.592$ (shown in Table 3) (Xiao and Yan, 2017). However, other researchers quoted the fulfilment of $0.813 < t < 1.107$ and $0.4 < \mu < 0.8$ criteria for stable perovskite and octahedral structures respectively (Park, 2015; Li et al., 2008).

To find out the structural stability of $CH_3NH_3PbI_3$ the Goldschmidt's tolerance factors and octahedral factor is calculated. The effective radii of $(CH_3NH_3)^+$, Pb^{+2} and I^- in the perovskite-type lattice is 2.1926 Å, 1.19 Å, and 2.20 Å, respectively using VESTA package (Momma and Izumi, 2011). The Goldschmidt tolerance factor is found to be 0.916 for $CH_3NH_3PbI_3$ and octahedral factor is 0.54.

Further, stability issue can also be resolved by calculating the formation energy of structures, which is defined as (Liu et al., 2018):

$$E_{formation} = (E_{total} - \sum_J n_j E_{ion}^j) \Big/ N_{total} \tag{3}$$

where E_{total} is the total energy of perovskite material and E_{ion}^j is the energy of the constituent elements in their respective elemental state, n_j is the number of various constituent elements, and N_{total} is the total number of atoms in unit cell (Liu et al., 2018). Lower value of formation energy indicates that the lattice is exothermic and more stable. Here the formation energy is found to be –0.42 eV/atom. The negative value of formation

energy shows that equation is exothermic and the energy of compound is less than that of constituent elements. This compound has stable bonds.

Table 3 Goldschmidt tolerance factor, octahedral factor and formation energy of $CH_3NH_3PbI_3$ perovskite

Goldschmidt tolerance factor	*Octahedral factor*	*Formation energy* (eV/atom)	*Reference*
0.91	0.54	–0.42	This work
0.83	–	–	Xiao and Yan (2017) and Green et al. (2014)
1.02	–	–	Liu et al. (2018)
0.95	–	–	Travis et al. (2016)
0.91	–	–	Kieslich et al. (2014)

3.3 Optical properties

The renewable energy production of novel devices can be determined by a detailed study of optical properties of these materials. In a macroscopic view, the interaction of matter with electromagnetic radiation can be described by Maxell's equations. These equations consider the specific constants as important parameters for optical properties of the material. These characteristic constant is permittivity, permeability and refractive indices which in fact are functions of frequency. The dielectric function in real is a complex variable of frequency and can be represented in the following manner:

$$\varepsilon(\omega) = \varepsilon_1(\omega) + i\varepsilon_2(\omega) \tag{4}$$

The imaginary part of the dielectric function $\varepsilon_2(\omega)$ can be calculated from the momentum matrix elements between the wave functions for occupied and unoccupied levels and is given by (Shi et al., 2015).

$$\varepsilon_2(\omega) = \frac{2\pi^2 e^2}{\Omega\varepsilon_0} \sum_{i\in c, f\in \upsilon} \sum_{k} \left| < \Psi_k^{\,c} \left| \hat{\mu} \bullet r \right| \Psi_k \upsilon \right|^2 \delta\left[E_k^{\,c} - E_k^{\,\upsilon} - \hbar\omega\right] \tag{5}$$

Here, ω, e, Ω are the phonon frequency, the electronic charge, and the volume of a unit cell respectively. μ denotes the unit vector along the polarisation of the incident electric field, $\Psi_k^{\,c}$ and $\Psi_k^{\,v}$ are the conduction band wave functions and valence band wave functions respectively at a particular k.

The Kramer-Kronig relations provide the real part $\varepsilon_1(\omega)$, which is evaluated from $\varepsilon_2(\omega)$ and is given by

$$\varepsilon_1(\omega) = 1 + \left(\frac{2}{\pi}\right) \int_0^\infty \frac{\omega'^2 \varepsilon_2(\omega')}{\omega'^2 - \omega^2} d\omega' \tag{4}$$

…

The optical properties; the absorption coefficient $\alpha(\omega)$, the refractive index $n(\omega)$, the extinction coefficient, the optical conductivity $\sigma(\omega)$, the reflectivity $R(\omega)$, and the loss

function is calculated from the real and imaginary parts of the dielectric function (Kojima et al., 2009; Amnuyswata and Thanomngam, 2017; Ogomi et al., 2014).

The real and imaginary parts of the dielectric function are displayed in Figure 5(a) and (b) respectively, for the photon energy ranging up to 14 eV. The main peak of the real part of the dielectric function appears at 2.08 eV. This dominated transition occurs due to electronic transitions from the upper valence band to the bottom part of the conduction band and further the spectra decreases up to 13.6 eV. The roots of $\varepsilon_1(\omega)$ are found in the energies 3.50 eV and 7.90 eV. These root values of $\varepsilon_1(\omega)$ has a physical significance of representing energy loss at these energies. Consequently, these energy values correspond to high absorption (Figure 6(a)). Moreover, within the energy regions between 8eV- 13.6 eV, the real part of dielectric function is negative showing that in this region of energy, wave propagation through the matter is not possible.

Figure 5 The calculated: (a) real $\varepsilon_1(\omega)$ and (b) imaginary $\varepsilon_2(\omega)$ parts of complex dielectric function for $CH_3NH_3PbI_3$ (see online version for colours)

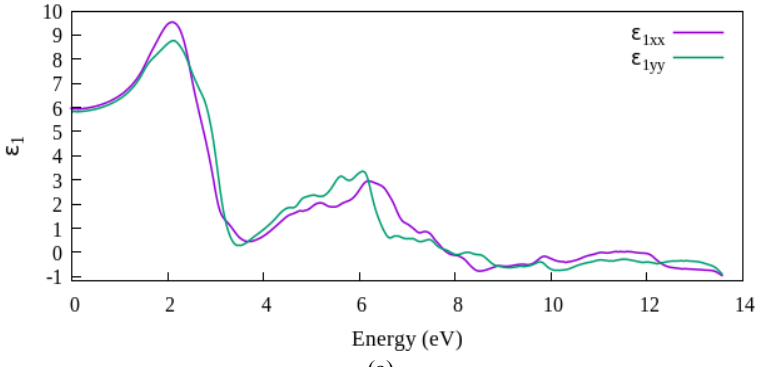

(a)

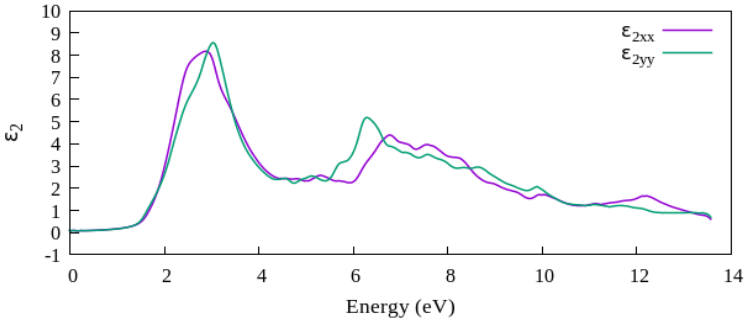

(b)

The imaginary part of the dielectric constant $\varepsilon_2(\omega)$ is another important factor for determining optical properties of materials. According to Figure 5(b), the first significant alteration in $\varepsilon_2(\omega)$ occurs at energy corresponding to 1.52 eV. This energy is required for the first direct optical transition and known as the optical gap. Here two prominent peaks arise at energies 3.03 eV and 6.29 eV. The inter band transitions of electrons are

responsible for the first prominent peak of the curve. These transitions take place from I-5p and Pb–6s occupied levels of valence bands to Pb-6p unoccupied levels of the conduction band. Also, there are transitions of electrons from the semi-core states in the conduction band; these transitions are responsible for the peaks at lower intensities. Also the static dielectric constant is calculated which is found to be 6 in good agreement with other workers (Yuan et al., 2015).

The optical absorption curve for $CH_3NH_3PbI_3$cubic perovskite in the bulk phase, using LDA approximation is shown in Figure 6 (a). The absorption edge starts from the optical band gap 1.52 eV, and is found corresponding to the direct R-R transition. Moreover, there is the existence of two minima in the curve of $\varepsilon_1(\omega)$ within energy range 3–9 eV (Figure 5(a)); two absorption peaks arises in this region (Figure 6(a)). The first peak lies in the range of visible light and placed at the energy 3.21 eV; this inference that significant absorption is being done by the compound in the visible range; this process grows within the ultraviolet region as absorption peak with 6.55 eV, occurs in UV region. This compound shows rather good absorption coefficient in the 8-14 eV region.

Figure 6 The calculated: (a) absorption coefficient; (b) reflectivity; (c) electron energy loss function and (d) photoconductivity for $CH_3NH_3PbI_3$ in cubic phase (see online version for colours)

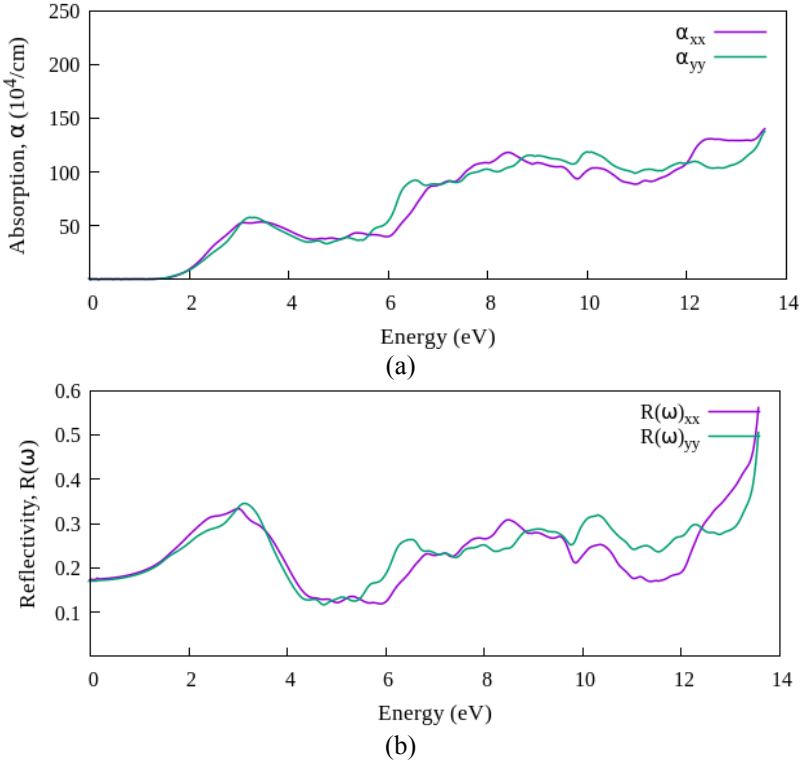

Figure 6 The calculated: (a) absorption coefficient; (b) reflectivity; (c) electron energy loss function and (d) photoconductivity for $CH_3NH_3PbI_3$ in cubic phase (see online version for colours) (continued)

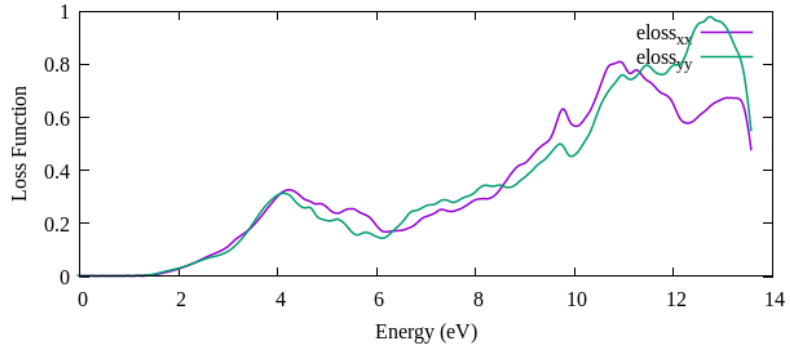

(c)

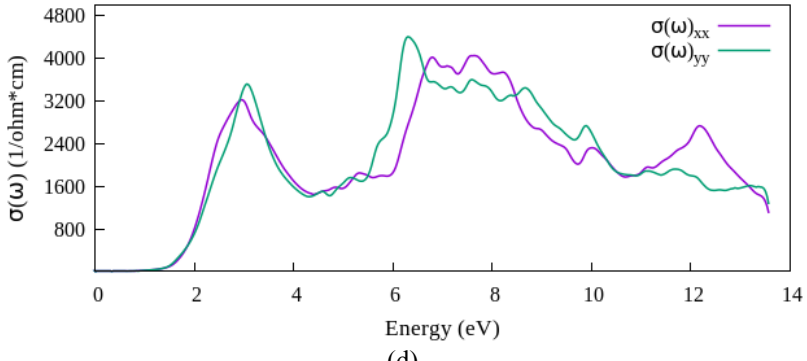

(d)

The refractive index is a complex function and it has its significance in explaining the propagation, dispersion and dissipation of electromagnetic waves. The $n(\omega)$, which is the real part of refractive index and imaginary part which is known as extinction coefficient are plotted in Figure 7.

The refractive index curve (Figure 7(a)) starts with the value 2.42 eV at zero energy, the static refractive index. It is also seen that with the increase in energy of radiation, refractive index increases, providing the peak at energy 2.24 eV with value 3.18 value of refractive index. The maximum value of refractive index lies in between 2–4 eV, within visible energy range. Further the difference in values of components of refractive indices in the perpendicular direction is 0.02 eV, which is very small; it confirms the isotropic behaviour of material in terms of optical properties.

The extinction coefficient for $CH_3NH_3PbI_3$ with respect to light energy is plotted in Figure 7(b). The highest maximum of the curve appears at energy 3.18 eV and the extinction coefficient is found to be 1.78. This result represents that near this range of energy, major amounts of absorption occurs and this has also been confirmed from the absorption peak in Figure 6(a). Also the first minimum is found at energy 5.51 eV, i.e., the absorption of rays of these energies is minimised. The same fact is founded from the absorption coefficient curve (Figure 6(a)). Moreover, large amounts of extinction coefficient are found in the infrared as well as in the visible region (1.5–3eV); and the absorption coefficient is large enough; this refers to the fact that radiation is absorbed in

sufficient amount, but electrons do not get enough energy for inter band transitions rather radiation may heat the crystal to produce plasmon fluctuations (Afsari et al., 2016).

Figure 7 (a) Refractive index $n(\omega)$ and (b) extinction coefficient vs. photon energy for cubic perovskite $CH_3NH_3PbI_3$ (see online version for colours)

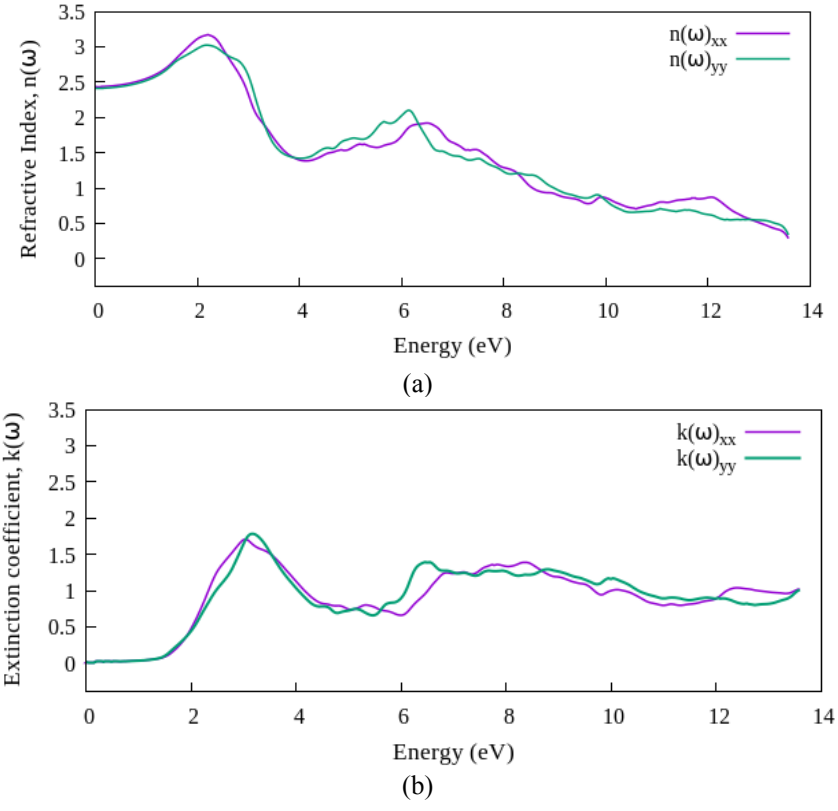

The electron energy loss function is an important optical parameter the loss function represents the loss of energy per unit length for a fast electron traversing in a material. Figure 6(c) shows the energy loss function as a function of photon energy. The peaks represent the highest loss at the particular energy which is due to collective oscillations of electrons and correspond to plasmon frequency. The comparison of peaks of loss function with the roots of the real dielectric function provide the plasma oscillation energy which is about 3.5 eV. Also the prominent peak of the curve at 3.9 eV, which correspond to energies of abrupt reduction in reflectivity (Figure 6(b)). Thus we conclude that the energy at which the real part $\varepsilon_1(\omega)$ of the dielectric function vanishes corresponds to the sharp drop in reflectivity curve and the prominent peak in energy loss curve.

Further the optical conductivities of $CH_3NH_3PbI_3$ material are shown in Figure 6(c). The optical conductivity is related to the photo-electric conversion efficiency. Here it is clear that maximum photoconductivity of the material lies within the UV range of energy; however peak in the visible region (3.8 eV) is also there, which confirms the reliability of $CH_3NH_3PbI_3$ material for the solar cell absorption layer.

4 Conclusion

In summary, in this work we have investigated the structural, electronic and optical properties of $CH_3NH_3PbI_3$ perovskite by performing the local density approximation (LDA) within the frame of density functional theory. The calculated lattice parameters are found in good agreement with experimental results. The electronic band gap is found to be 1.52 eV at the R-R transition and density of state curves show that the electronic properties of the material are determined by distortion of PbI_6 octahedral rather than direct involvement of CH_3NH_3 molecule. The optical properties, i.e., dielectric function, reflectivity, optical conductivity, absorption coefficient are discussed within 0–14 eV energy range. The energy at which the real part of the dielectric function vanishes corresponds to the sharp drop in reflectivity curve and the prominent peak in the energy loss curve. Also, the stability of the structure is confirmed by considering stability criteria of Goldsmith tolerance factor and formation energy. The structural, electronic and optical properties as well as structural stability confirm the potential use of $CH_3NH_3PbI_3$material as an absorption layer in solar cell application.

References

Afsari, M., Boochani, A. and Hantezadeh, M. (2016) 'Electronic, optical and elastic properties of cubic perovskite $CsPbI_3$□: using first principles study', *Optik – International Journal for Light and Electron Optics*, Vol. 127, pp.11433–11443.

Amnuyswata, K. and Thanomngam, P. (2017) 'Effect of exchange-correlation and GW approximations on electrical property of cubic, tetragonal and orthorhombic $CH_3NH_3PbI_3$', *Integrated Ferroelectrics*, Vol. 117, pp.1–9.

Baikie, T., Fang, Y., Kadro, J.M., Schreyer, M., Wei, F., Mhaisalkar, S.G., Graetzel, M. and White, T.J. (2013) 'Synthesis and crystal chemistry of the hybrid perovskite $(CH_3NH_3)PbI_3$ for solid-state sensitised solar cell applications', *Journal of Materials Chemistry A*, Vol. 1, p.5628.

Bartel, C.J., Sutton, C., Goldsmith, B.R., Ouyang, R., Musgrave, C.B., Ghiringhelli, L.M. and Scheffler, M. (2019) 'New tolerance factor to predict the stability of perovskite oxides and halides', *Science Advances*, Vol. 5, No. 2, pp.1–9.

Bing, J., Kim, J., Zhang, M., Zheng, J., Lee, D.S., Cho, Y., Deng, X., Lau, C.F.J., Li, Y., Green, M.A., Huang, S. and Ho-Baillie, A. (2019) 'The impact of a dynamic two-step solution process on film formation of $Cs_{0.15}(MA_{0.7}FA_{0.3})_{0.85}PbI_3$ perovskite and solar cell performance', *Small*, Vol. 15, No. 9, pp.1–15.

Bing, J., Lee, D.S., Zheng, J., Zhang, M., Li, Y., Kim, J., Lau, C.F.J., Cho, Y., Green, M.A., Huang, S. and Ho-Baillie, A.W.Y. (2019) 'Deconstruction-assisted perovskite formation for sequential solution processing of $Cs_{0.15}(MA_{0.7}FA_{0.3})_{0.85}PbI_3$ solar cells', *Solar Energy Materials and Solar Cells*, Vol. 203, p.110200.

Blaha, P., Schwarz, K., Madsen, G.K.H., Kvasnicka, D., Luitz, J., Laskowsk, R., Tran, F., Marks, L. and Marks, L. (2019) *Karlheinz Schwarz/Techn*, Universität Wien, Austria.

Chen, G., Seo, J., Yang, C. and Prasad, P.N. (2003) 'Nanochemistry and nanomaterials for photovoltaics', *Chemical Society Reviews*, Vol. 42, pp.8304–8338.

Egger, D.A. and Kronik, L. (2014) 'Role of dispersive interactions in determining structural properties of organic–inorganic halide perovskites: insights from first-principles calculations', *The Journal of Physical Chemistry Letters*, Vol. 5, pp.2728–2733.

Feng, J. (2014) 'Mechanical properties of hybrid organic-inorganic $CH_3NH_3BX_3$ (B = Sn, Pb; X = Br, I) perovskites for solar cell absorbers', *APL Materials*, Vol. 2, No. 8, p.081801.

Gao, P., Grätzel, M. and Nazeeruddin, M.K. (2014) 'Organohalide lead perovskites for photovoltaic applications', *Energy Environ. Science*, Vol. 7, pp.2448–2463.

Goldschmidt, V.M. (1926) 'Die gesetze der krystallochemie', *Die Naturwissenschaften*, Vol. 14, pp.477–485.

Green, M.A., Ho-Baillie, A. and Snaith, H.J. (2014) 'The emergence of perovskite solar cells', *Nature Photonics*, Vol. 8, pp.506–514.

Hagfeldt, A., Boschloo, G., Sun, L., Kloo, L. and Pettersson, H. (2010) 'Dye-sensitized solar cells', *Chemical Reviews*, Vol. 110, pp.6595–6663.

Hao, F., Stoumpos, C.C., Chang, R.P.H. and Kanatzidis, M. (2014) 'Anomalous band gap behavior in mixed Sn and Pb perovskites enables broadening of absorption spectrum in solar cells', *Journal of the American Chemical Society*, Vol. 136, pp.8094–8099.

Hemant Kumar, M., Yantara, N., Dharani, S., Graetzel, M., Mhaisalkar, S., Boix, P.P. and Mathews, N. (2013) 'Flexible, low-temperature, solution processed ZnO-based perovskite solid state solar cells', *Chemical Communications*, Vol. 49, p.11089.

Huang, L., Cui, X., Liu, C., Yang, W., Shi, W., Lai, J. and Wang, L. (2020) 'Improvement on performance of hybrid $CH_3NH_3PbI_{3-x}Cl_x$ perovskite solar cells induced sequential deposition by low pressure assisted solution processing', *Solar Energy*, Vol. 199, pp.826–831.

Indari, E.D., Wungu, T.D.K. and Hidayat, R. (2017) 'Ab-initio calculation of electronic structure of lead halide perovskites with formamidinium cation as an active material for perovskite solar cells', *Journal of Physics: Conference Series*, Vol. 877, p.012054.

Jishi, R.A., Ta, O.B. and Sharif, A.A. (2014) 'Modeling of lead halide perovskites for photovoltaic applications', *The Journal of Physical Chemistry C*, Vol. 118, pp.28344–28349.

Juarez-Perez, E.J., Sanchez, R.S., Badia, L., Garcia-Belmonte, G., Kang, Y.S., Mora-Sero, I. and Bisquert, J. (2014) 'Photoinduced giant dielectric constant in lead halide perovskite solar cells', *The Journal of Physical Chemistry Letters*, Vol. 5, pp.2390–2394.

Kieslich, G., Sun, S. and Cheetham, A.K. (2014) 'Solid-state principles applied to organic–inorganic perovskites: new tricks for an old dog', *Chem. Science*, Vol. 5, pp.4712–4715.

Kim, H-S., Lee, C-R., Im, J-H., Lee, K-B., Moehl, T., Marchioro, A., Moon, S-J., Humphry-Baker, R., Yum, J-H., Moser, J.E., Gratzel, M. and Park, N-G. (2012) 'Lead iodide perovskite sensitized all-solid-state submicron thin film mesoscopic solar cell with efficiency exceeding 9%', *Scientific Reports*, Vol. 2, p.501.

Kim, J., Lee, S-H., Lee, J.H. and Hong, K-H. (2014) 'The role of intrinsic defects in methylammonium lead iodide pervoskite', *J. Phys Chem Lett.*, Vol. 5, pp.1312–1317.

Kojima, A., Teshima, K., Shirai, Y. and Miyasaka, T. (2009) 'Organometal halide perovskites as visible-light sensitizers for photovoltaic cells', *Journal of the American Chemical Society*, Vol. 131, pp.6050–6051.

Kulkarni, S.A., Baikie, T., Boix, P.P., Yantara, N., Mathews, N. and Mhaisalkar, S. (2014) 'Band-gap tuning of lead halide perovskites using a sequential deposition process', *J. Mater. Chem.A.*, Vol. 2, pp.9221–9225.

Li, C., Lu, X., Ding, W., Feng, L., Geo, Y. and Guo, Z. (2008) 'Formability of ABX3 (X = F, Cl, Br, I) halide perovskites', *Acta Crystallogr. B.*, Vol. 64, pp.702–707.

Lind, H., Wilson, J. and Mather, R. (2011) 'Raman spectroscopy of thin-film silicon on woven polyester', *Physica Status Solidi a-Applications and Materials Science*, Vol. 208, pp.2765–2771.

Liu, D., Li, S., Bian, F. and Meng, X. (2018) 'First-principles investigation on the electronic and mechanical properties of Cs-doped $CH_3NH_3PbI_3$', *Materials*, Vol. 11, No. 7, pp.1–11.

Madsen, G.K.H., Blaha, P., Schwarz, K., Sjöstedt, E. and Nordström, L. (2001) 'Efficient linearization of the augmented plane-wave method', *Physical Review B*, Vol. 64, No. 19, pp.195134–195139.

Momma, K. and Izumi, F. (2011) 'VESTA3 for three-dimensional visualization of crystal, volumetric and morphology data', *Journal of Applied Crystallography*, Vol. 44, pp.1272–1276.

Monkhorst, H.J. and Pack, J.D. (1976) 'Special points for Brillouin-zone integrations', *Physical Review B*, Vol. 13, pp.5188–5192.

Mosconi, E., Amat, A., Nazeeruddin, M.K., Grätzel, M. and De Angelis, F. (2013) 'First-principles modeling of mixed halide organometal perovskites for photovoltaic applications', *The Journal of Physical Chemistry C*, Vol. 117, No. 27, pp.13902–13913.

Najafi, L., Taheri, B., Martín-García, B., Bellani, S., Di Girolamo, D., Agresti, A., Oropesa-Nuñez, R., Pescetelli, S. and Vesce, L., Calabro, E., Prato, M., Del Rio Castillo, A.E., Carlo, A.D. and Bonaccorso, F. (2018) 'MoS_2 quantum dot/graphene hybrids for advanced interface engineering of a $CH_3NH_3PbI_3$ perovskite solar cell with an efficiency of over 20%', *ACS NaNo,* Vol. 12, pp.10736–10754.

Ogomi, Y., Morita, A., Tsukamoto, S., Saitho, T., Fujikawa, N., Shen, Q., Toyoda, T., Yoshiissue K., Pandey, S.S., Ma, T. and Hayase, S. (2014) '$CH_3NH_3SnxPb(1–x)I_3$ perovskite solar cells covering up to 1060 nm', *The Journal of Physical Chemistry Letters*, Vol. 5, pp.1004–1011.

Onoda-Yamamuro, N., Matsuo, T. and Suga, H. (1990) 'Calorimetric and IR spectroscopic studies of phase transitions in methylammonium trihalogenoplumbates (II)', *Journal of Physics and Chemistry of Solids*, Vol. 51, pp.1383–1395.

Park, N-G. (2015) 'Perovskite solar cells: an emerging photovoltaic technology', *Materials Today*, Vol. 18, pp.65–72.

Perdew, J.P., Burke, K. and Ernzerhof, M. (1996) 'Generalized gradient approximation made simple', *Physical Review Letters*, Vol. 77, pp.3865–3868.

Poglitsch, A. and Weber, D. (1987) 'Dynamic disorder in methylammoniumtrihalogenoplumbates (II) observed by millimetre-wave spectroscopy', *The Journal of Chemical Physics*, Vol. 87, pp.6373–6378.

Ponseca, C.S., Savenije, T.J., Abdellah, M., Zheng, K., Yartsev, A., Pascher, T., Harlang, T., Chabera, P., Pullerits, T., Stepanov, A., J-P. and Sundström, V. (2014) 'Organometal halide perovskite solar cell materials rationalized: ultrafast charge generation, high and microsecond-long Balanced mobilities, and slow recombination', *Journal of the American Chemical Society*, Vol. 136, pp.5189–5192.

Prakash Singh, S. and Nagarjuna, P. (2014) 'Organometal halide perovskites as useful materials in sensitized solar cells', *Dalton Transactions*, Vol. 43, pp.5247–5251.

Roknuzzaman, M., Ostrikov, K., Wasalathilake, K.C., Yan, C., Wang, H. and Tesfamichael, T. (2018) 'Insight into lead-free organic-inorganic hybrid perovskites for photovoltaics and optoelectronics: A first-principles study', *Organic Electronics*, Vol. 59, pp.99–106.

Ryu, S., Noh, J.H., Jeon, N.J., Kim, Y.C., Yang, W.S., Seo, J. and Seok, S.I. (2014) 'Voltage output of efficient perovskite solar cells with high open-circuit voltage and fill factor', *Energy Environ. Sci.*, Vol. 7, pp.2614–2618.

Schwarz, K., Blaha, P. and Madsen, G.K.H. (2002) 'Electronic structure calculations of solids using the WIEN2k package for material sciences', *Computer Physics Communications*, Vol. 147, pp.71–76.

Shah, A.V., Schade, H., Vanecek, M., Meier, J., Vallat-Sauvain, E., Wyrsch, N., Kroll, U., Droz, C. and Bailat, J. (2014) 'Thin-film silicon solar cell technology', *Progress in Photovoltaics: Research and Applications*, Vol. 12, pp.113–142.

Shi, D., Adinolfi, V., Comin, R., Yuan, M., Alarousu, E., Buin, A., Chen, Y., Hoogland S., Rothenberger, A., Katsiev, K., Losovyj, Y., Zhang, X., Dowben, P.A., Mohammed, O.F., Sargent, E.H. and Bakr, O.M. (2015) 'Low trap-state density and long carrier diffusion in organolead trihalide perovskite single crystals', *Science*, Vol. 347, pp.519–522.

Singh, S., Shourie, R.J. and Kabra, D. (2019) 'Efficient and thermally stable $CH_3NH_3PbI_3$ based perovskite solar cells with double electron and hole extraction layers', *Journal of Physics D: Applied Physics*., Vol. 52, No. 25, p.255106.

Stoumpos, C.C., Malliakas, C.D. and Kanatzidis, M.G. (2003) 'Semiconducting tin and lead iodide perovskites with organic cations: phase transitions, high mobilities, and near-infrared photoluminescent properties', *T Inorganic Chemistry*, Vol. 52, No. 15, pp.9019–9038.

Thind, A.S., Huang, X., Sun, J. and Mishra, R. (2017) 'First-principles prediction of a stable hexagonal phase of $CH_3NH_3PbI_3$', *Chemistry of Materials*, Vol. 29, pp.6003–6011.

Tonui, P., Oseni, S.O., Sharma, G., Yan, Q. and Mola, G.T. (2018) 'Perovskites photovoltaic solar cells: An overview of current status', *Renewable and Sustainable Energy Reviews*, Vol. 91, pp.1025–1044.

Tran, F., Laskowski, R., Blaha, P. and Schwarz, K. (2007) 'Performance on molecules, surfaces, and solids of the Wu-Cohen GGA exchange-correlation energy functional', *Physical Review B*, Vol. 75, No. 11, p.115131.

Travis, W., Glover, E.N.K., Bronstein, H., Scanlon, D.O. and Palgrave, R.G. (2016) 'On the application of the tolerance factor to inorganic and hybrid halide perovskites: a revised system', *Chemical Science*, Vol. 7, pp.4548–4556.

Tyuterev, V.G. and Vast, N. (2006) 'Murnaghan's equation of state for the electronic ground state energy', *Computational Materials Science*, Vol. 38, pp.350–353.

Umari, P., Mosconi, E. and De Angelis, F. (2014) 'Relativistic GW calculations on $CH_3NH_3PbI_3$ and $CH_3NH_3SnI_3$ perovskites for solar cell applications', *Scientific Reports*, Vol. 4, p.4467.

Umebayashi, T., Asai, K., Kondo, T. and Nakao, A. (2003) 'Electronic structures of lead iodide based low-dimensional crystals', *Physical Review B*, p.155405.

Wang, K-C., Jeng, J-Y., Shen, P-S., Chang, Y-C., Diau, E.W-G., Tsai, C-H., Chao, T-Y., Hsu, H-C., Lin, P.Y., Chen, P. and Guo, T-F. and Wen, T-C. (2014) 'P-type mesoscopic nickel oxide/organometallic perovskite heterojunction solar cells', *Scientific Reports*, Vol. 4, p.4756.

Weber, D. (1978) '$CH_3NH_3PbX_3$, ein Pb(II)-System mit kubischer Perowskitstruktur', *TZeitschrift Fur Naturforschung B*, Vol. 33, pp.1443–1445.

Wu, Z. and Cohen, R.E. (2006) 'More accurate generalized gradient approximation for solid', *Physical Review B*, Vol. 73, p.235116.

Xiao, Z. and Yan, Y. (2017) 'Progress in theoretical study of metal halide perovskite solar cell materials', *Advanced Energy Materials*, Vol. 7, p.1701136.

Yang, W.S., Park, B-W., Jung, E.H., Jeon, N.J., Kim, C., Lee, Y.D.U., Shin, S.S., Seo, J., Kim, E.K., Noh, J.H. and Seok, S.I. (2017) 'Iodide management in formamidinium-lead-halide–based perovskite layers for efficient solar cells', *Science*, Vol. 356, pp.1376–1379.

Yin, W-J., Shi, T. and Yan, Y. (2014) 'xxxx', *Applied Physics Letters*, Vol. 104, p.063903.

Yin, W-J., Yang, J-H., Kang, J., Yan, Y. and Wei, S-H. (2015) 'Halide perovskite materials for solar cells: a theoretical review', *Journal of Materials Chemistry A*, Vol. 3, pp.8926–8942.

Yuan, F., Wu, Z., Dong, H., Xia, B., Xi, J., Ning, S. and Hou, X. (2015) 'Electric field-modulated amplified spontaneous emission in organo-lead halide perovskite $CH_3NH_3PbI_3$', *Applied Physics Letters*, Vol. 107, p.261106.

Yun, J.S., Kim, J., Young, T., Patterson, R.J., Kim, D., Seidel, J., Lim, S., Green, M.A., Huang, S. and Ho-Baillie, A. (2018) 'Humidity-induced degradation via grain boundaries of $HC(NH_2)_2$ PbI_3 planar perovskite solar cells', *Advanced Functional Materials*, Vol. 28, p.1705363.